Crystal structure of an ACh-binding protein reveals the ligand-binding domain of nicotinic receptors

Katjuša Brejc*, Willem J. van Dijk*, Remco V. Klaassen†, Mascha Schuurmans†, John van der Oost†‡, August B. Smit† & Titia K. Sixma*

* Division of Molecular Carcinogenesis, Netherlands Cancer Institute, Plesmanlaan 121, 1066 CX Amsterdam, The Netherlands
† Department of Molecular and Cellular Neurobiology, Research Institute Neurosciences Vrije Universiteit, Faculty of Biology, De Boelelaan 1087, 1081 HV Amsterdam, The Netherlands

....

Pentameric ligand gated ion-channels, or Cys-loop receptors, mediate rapid chemical transmission of signals. This superfamily of allosteric transmembrane proteins includes the nicotinic acetylcholine (nAChR), serotonin 5-HT$_3$, γ-aminobutyric-acid (GABA$_A$ and GABA$_C$) and glycine receptors. Biochemical and electrophysiological information on the prototypic nAChRs is abundant but structural data at atomic resolution have been missing. Here we present the crystal structure of molluscan acetylcholine-binding protein (AChBP), a structural and functional homologue of the amino-terminal ligand-binding domain of an nAChR α-subunit. In the AChBP homopentamer, the protomers have an immunoglobulin-like topology. Ligand-binding sites are located at each of five subunit interfaces and contain residues contributed by biochemically determined 'loops' A to F. The subunit interfaces are highly variable within the ion-channel family, whereas the conserved residues stabilize the protomer fold. This AChBP structure is relevant for the development of drugs against, for example, Alzheimer's disease and nicotine addiction.

....

The superfamily of pentameric ligand-gated ion channels (LGICs), including nAChR, 5-HT$_3$, GABA$_A$ and GABA$_C$, and glycine receptors, mediates chemical synaptic transmission. All of these LGICs form homo- or heteropentamers of related subunits, implying a common evolutionary origin[1]. Each subunit is divided into an N-terminal or ligand-binding domain (LBD), a transmembrane region and an intracellular region[2]. The LBDs, which are around 210 amino-acid residues long, contain ligand-binding sites for agonists and competitive antagonists. Binding of an agonist induces rapid opening of the transmembrane ion channel, leading to a change in membrane potential. The signal transmission mechanism is explained by allosteric interactions between subunits, involving numerous conformational transitions[3,4].

The nAChRs are extensively studied and can be divided into muscle and neuronal types[2]. The muscle type, with stoichiometry $(\alpha_1)_2\beta_1\gamma\delta$, is found at the neuromuscular junction and in the electric organs of fish such as the electric ray *Torpedo californica*. It presents a common drug target for muscle relaxants. The neuronal nAChRs, which are hetero- or homomeric (for example, $(\alpha_4)_2(\beta_2)_3$ or $(\alpha_7)_5$), are located on both pre- and postsynaptic nerve terminals. They are important drug targets as they mediate nicotine addiction in smokers and the positive effects of nicotine on cognition, memory and attention in patients with, for example, schizophrenia or Alzheimer's and Parkinson's diseases[5].

In nAChRs, the ligand-binding site is located at the interface between two subunits[2,4]. Numerous biochemical studies showed that the principal part is always formed by the α-subunit residues—contributing to the so-called 'loops' A (ref. 6), B (ref. 7) and C (refs 7–10)—whereas the neighbouring subunit residues—contributing to the 'loops' D (refs 11, 12), E (refs 10, 13) and F (refs 14–16)—form the complementary part of the binding pocket. Thus, the muscle nAChR contains two different ligand-binding sites ($\alpha_1\delta$ and $\alpha_1\gamma$) with distinct affinities, whereas the homopentameric α_7 receptor contains five identical ligand-binding sites. In these sites

acetylcholine is expected to bind through cation-π interactions, where the positive charge of the quaternary ammonium of acetylcholine interacts with the electron-rich aromatic side chains[17].

So far, the only experimental structural information on the nAChRs came from electron microscopy studies on *Torpedo* receptors[18–20]. These low–medium-resolution studies revealed the overall shape and dimensions of the receptor, a location of the ligand-binding site and the organization of the ion channel. The most recent 4.6 Å data[21] showed acetylcholine-binding pockets surrounded by seven-stranded β-sheet structures. This fits with circular dichroism measurements demonstrating that LBDs are predominantly β-structured[22–24]. No high-resolution data are available yet and although soluble LBDs have been produced[22–26], protein quantities were insufficient for high-resolution studies.

Acetylcholine-binding protein

Acetylcholine-binding protein (AChBP) is a soluble protein found in the snail *Lymnaea stagnalis*[27]. It is produced and stored in glial cells, and released in an acetylcholine-dependent manner into the synaptic cleft, where it modulates synaptic transmission. Mature AChBP is 210 residues long and forms a stable homopentamer. It aligns with the N-terminal domains of pentameric LGICs (Fig. 1) and lacks the transmembrane and intracellular domains present in the superfamily[27]. AChBP is most closely related to the α-subunits of the nAChRs (Fig. 1). Nearly all residues that are conserved within the nAChR family are present in AChBP, including those that are relevant for ligand binding. Moreover, AChBP binds known nAChR agonists and competitive antagonists such as acetylcholine, nicotine, *d*-tubocurarine and α-bungarotoxin[27]. Therefore, AChBP can be used as an example of the N-terminal domain of an α-subunit of nAChRs. Here we report the crystal structure of the AChBP homopentamer at 2.7 Å resolution.

Structure determination

The crystal structure of AChBP was solved using weak Pb multiple-wavelength anomalous diffraction (MAD) data in two crystal forms.

The electron density map was improved substantially by cross-crystal averaging of three crystal forms with 20, 10 and 5 copies of the protomer in the asymmetric unit (Table 1). The structure was refined at 2.7 Å in space group $P4_22_12$, with one AChBP pentamer in the asymmetric unit. Refinement with partial five-fold non-crystallographic symmetry (NCS) restraints resulted in an R-factor of 26.4% ($R_{free} = 30\%$).

The AChBP pentamer
The AChBP homopentamer, when viewed along the five-fold axis, resembles a windmill toy, with petal-like protomers (Fig. 2a). When viewed perpendicular to the five-fold axis it forms a 62-Å-high cylinder (Fig. 2b), with a diameter of 80 Å. The diameter of the central hole is ~18 Å, between side chains. These dimensions are in good agreement with the N-terminal domain in the Torpedo nAChR electron microscopy data[21]. In the pentamer the only subunit contacts are dimer interfaces, of which each protomer has two, the plus side and the minus side. We refer to the A (plus)−B (minus) interface as an example for the five equivalent interfaces AB, BC, CD, DE and EA (Fig. 2).

The AChBP protomer
Each AChBP protomer is a single domain protein, asymmetric in shape, with a size of around $62 \times 47 \times 34\ \text{Å}^3$ (Fig. 3a). It consists of an N-terminal α-helix, two short 3_{10} helices and a core of ten β-strands, which form a β-sandwich. The order of β-strands conforms
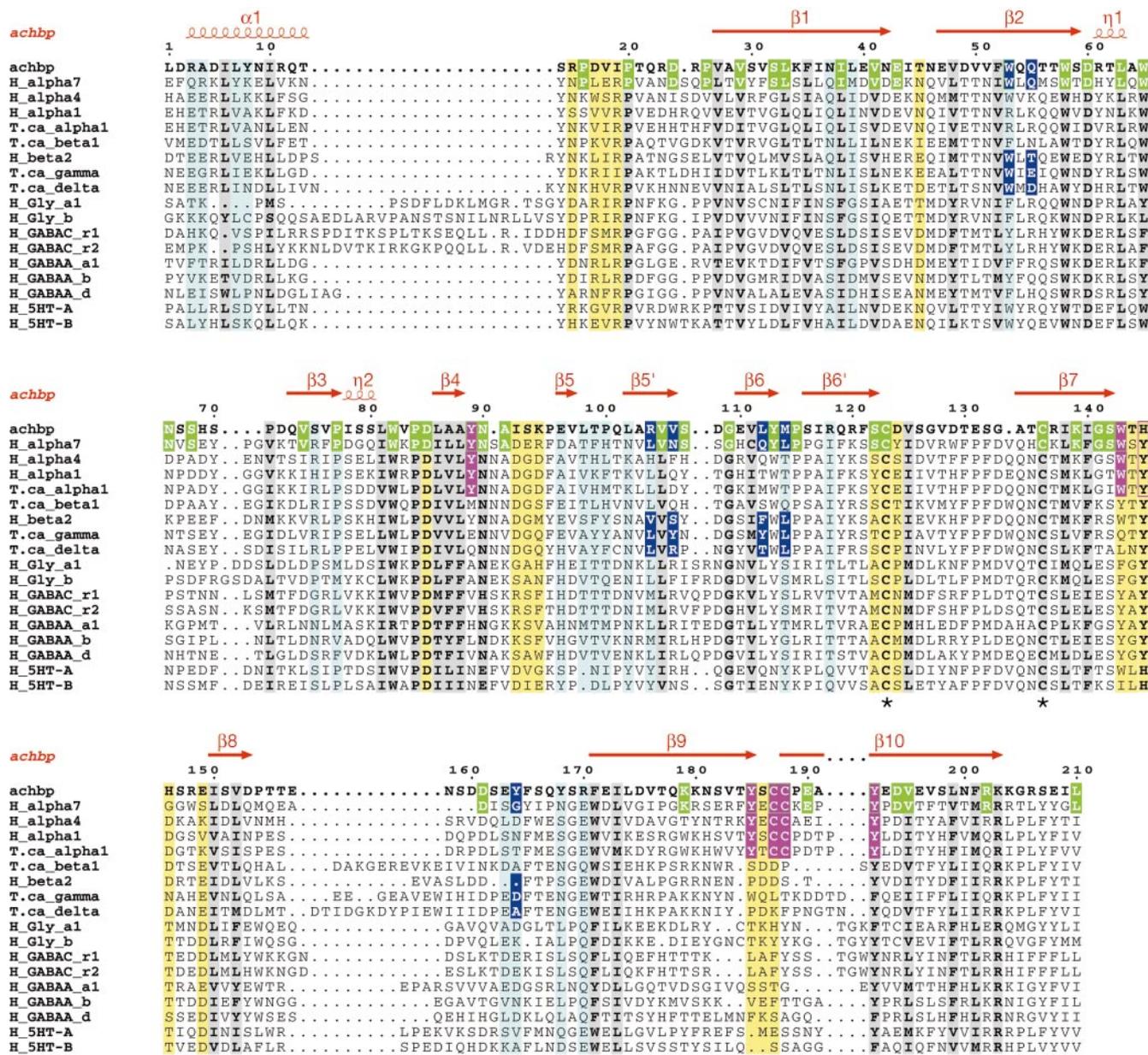
Figure 1 Sequence alignment of AChBP with pentameric ligand-gated ion channels (LGICs). The alignment shows only the N-terminal domain of the LGIC subunits and is based on a multi-sequence ClustalX[50] alignment of 92 full-length pentameric LGIC sequences. Alignments are shown from first to last AChBP residue (for example, starting at second residue of mature Torpedo α, $\beta\ \gamma$ and δ subunits, ending ~4 residues into the first transmembrane domain[29]). H: human, T.ca: Torpedo californica. Secondary structure elements (α: α-helix, β: β-strand, η: 3_{10}-helix) are indicated in red above the sequence, in accordance with Fig. 3a. Precise beginnings and ends will change with higher resolution. AChBP shares 24% sequence identity with the ligand-binding domain (LBD) of human α_7 (shown in green), 20–24% with other nicotinic receptors and 15–18% with other LGICs. The residues conserved in the superfamily are shown in bold with grey background. Asterisk, beginning and end of the Cys loop. Colouring of interface residues at the plus (yellow) and minus side (light blue) shows the lack of sequence conservation in the subunit interface across the pentameric LGIC family. Nicotinic receptor ligand-binding residues on the principal (pink) and complementary (dark blue) side are indicated.

Table 1 Data collection statistics

Data set	λ_1 peak	λ_2 remote	λ_3 infl.	λ_1 peak	λ_2 infl.	Native
Space group	$P2_12_12$			$P2_1$		$P4_22_12$
Resolution (Å)	3.3/3.4–3.3			3.0/3.1–3.0		2.7/2.8–2.7
Wavelength (Å)	0.9492	0.8610	0.9507	0.9479	0.9498	0.943
Completeness (%)	99.7/99.7	99.6/99.6	99.7/99.7	99.9/99.9	99.5/99.5	97.8/96.5
Mosaicity (deg.)	0.62			0.43		0.78
Redundancy	3.7/3.8	3.8/3.9	3.7/3.8	3.5/2.2	3.2/2.0	6.5
R_{merge} (%)	7.7/46.8	7.8/45.2	8.3/55.0	5.9/26.1	6.0/32.9	5.9/67.4
$I/\sigma I$	8.7/1.6	8.4/1.7	8.3/1.4	7.7/2.7	6.8/1.5	27.4/2.3
Phasing	ISO/ANO	ISO/ANO	ISO/ANO	ISO/ANO	ISO/ANO	
R_{cullis} (%)	0.74/0.89	n.a./0.92	0.54/0.94	n.a./0.74	0.66/0.77	
Phasing power	0.57/1.2	n.a./1.06	2.3/0.91	n.a./1.1	0.37/1.22	
Figure of merit (overall)	0.45			0.28		

$<I/\sigma I>$, Mean signal to noise, where I is the integrated intensity of a measured reflection and σI is the estimated error in the measurement; $R_{merge} = \Sigma_{hkl}\Sigma_i |I_i(hkl) - <I(hkl)>|/\Sigma_{hkl}\Sigma_i I_i(hkl)$; $R_{cullis} = \Sigma_{hkl}||F_{PH} + F_P| - F_H(calc)|/\Sigma_{hkl}|F_{PH} + F_P|$.
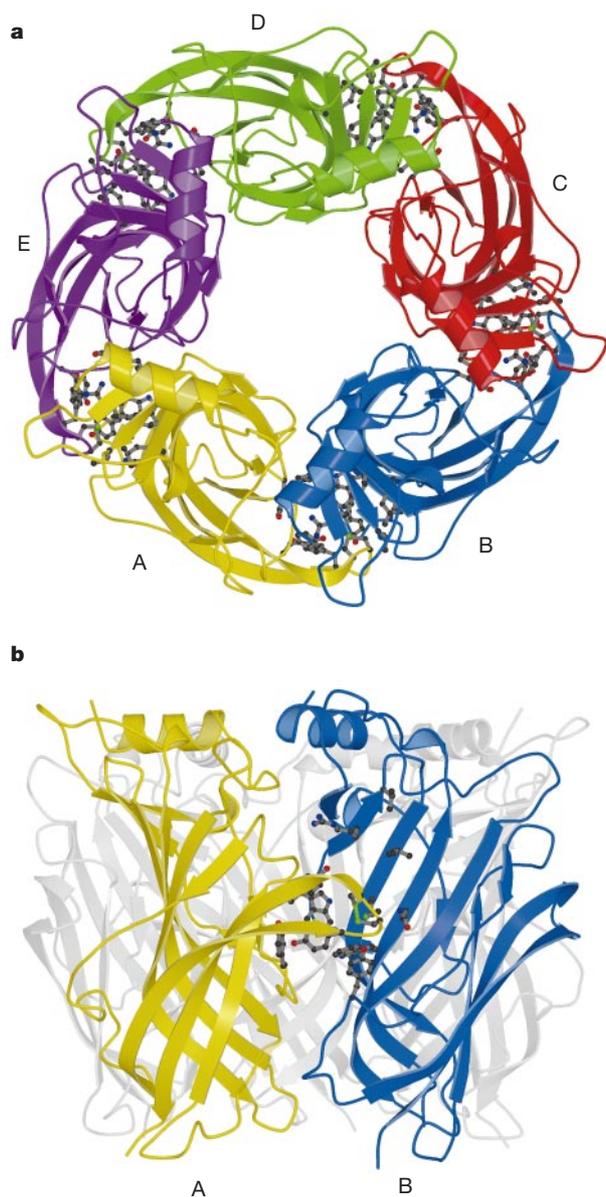
Figure 2 The pentameric structure of AChBP. **a**, In this representation each protomer has a different colour. Subunits are labelled anti-clockwise, with A–B, B–C, C–D, D–E and E–A forming the plus and minus interface side, with the principal and complementary ligand-binding sites, respectively (ball-and-stick representation). **b**, Viewing the AChBP pentamer perpendicular to the five-fold axis. The equatorially located ligand-binding site (ball-and-stick representation) is highlighted only in the A (yellow)–B (blue) interface.

to a modified immunoglobulin (Ig) topology[28] (Fig. 3b) with an extra β-hairpin (f′–f″) and an extra strand (b′). These additional strands introduce two 'Greek key' folding motifs. An Ig-like topology had been predicted for nAChRs[2,29], but the location of the ligand-binding site was missed, owing to the presence of extra β-strands. Compared with the classical Ig-fold[28], the AChBP β-strands are considerably twisted, with the β-sheets rotated against each other, resulting in two separate hydrophobic cores. Thus the three-dimensional fold does not resemble other Ig-like proteins and comparison[30] with the protein database did not result in a significant match to any known structure.

Positioning of functional regions

In the structure, the N and C termini are located at 'top' and 'bottom' of the pentamer, respectively. In the ion channels the transmembrane domains are at the C-terminal end of the LBD, at the 'bottom' of the AChBP structure (Figs 2b and 3), starting directly at the end of β-strand β10.

In muscle type nAChRs, the main immunogenic region (MIR), comprising residues $\alpha_1$67–$\alpha_1$76, acts as an epitope in the auto-immune disease myasthenia gravis[31]. Although the MIR-related region in AChBP (residues 65–72) has no sequence homology with the α_1-subunit, its location in a highly accessible position in loop L3 at the 'top' of the pentamer agrees with the expected accessibility for this region (Fig. 3a). It also fits with electron microscopy studies that located the MIR at the distal end of the receptor relative to the membrane[20].

The central pore of the pentamer is very hydrophilic, lined with charged residues. On each AChBP promoter, a large pocket is visible, accessible from the central pore. Each pocket, framed at the entrance by β-strands (β3, β4, β5 and β5′) (Fig. 3a), is uncharged and mainly hydrophobic. This region probably corresponds to the tunnel framed by twisted β-strands that was observed in the α_1-subunit of the *Torpedo* receptor at 4.6 Å resolution[21].

There is a different cavity at each interface between the subunits. These cavities are lined by residues, which were biochemically shown to be involved in ligand binding in nAChRs[2,5–16]. These cavities are mostly buried from the solvent, and located close to the outside of the pentameric ring (Fig. 2a). When viewed perpendicular to the five-fold axis, they are roughly equatorially positioned, about 30 Å away from the C termini (Fig. 2b), conforming to the expected location of the *Torpedo* receptor ligand-binding site, as determined by labelling[32] and electron microscopy studies[18]. We have concluded that these cavities are the ligand-binding sites.

The ligand-binding site

Each ligand-binding site is found in a cleft formed by a series of loops from the principal face of one subunit and a series of β-strands from the complementary face of an adjacent subunit (Fig. 4). The

principal side on the plus side of the AB interface consists of residues coming from loop A (Tyr A89), loop B (Trp A143, A145) and loop C (Tyr A185, the double cysteine A187−A188 and Tyr A192) (Fig. 4c). The complementary part of this binding side is formed by β-strands in protomer B contributing loop D (Trp B53, Gln B55), loop E (Arg B104, Val B106, Leu B112 and Met B114) and loop F (Tyr B164) (Fig. 4d). Four of the aromatic residues form the bottom half of the cavity (Tyr A89, Tyr A185, Tyr B164 and Trp B53). The walls are formed by Tyr A192, Trp A143, the main chain of A145, the side chains of Met B114 and Gln B55, and the vicinal disulphide (Cys A187−Cys A188). The hydrophobic parts of Arg B104, Val B106 and Leu B112 form the top of the binding site (Fig. 4a).

All residues in the binding site have been identified by photo-affinity labelling and mutagenesis studies[6–16]. Although the side chain of His A145 is pointing away from the cavity, its main chain is involved in the binding site. One residue identified by labelling studies[6], Trp A82 (α_1 Trp 86), is involved in hydrophobic core formation and located far from the pocket. Therefore it probably does not participate directly in ligand binding. Additional residues may be involved in binding large ligands such as toxins[13]. Otherwise, the AChBP ligand-binding site entirely confirms the available biochemical and mutational data on nAChRs. The structure, how-ever, reveals for the first time how these residues are positioned with respect to each other, and will provide a valuable tool for drug design studies.

All observed residues are conserved between known ligand-binding subunits of nicotinic receptors except the loop F Tyr B164 residue. In our structure the loop F region has an unusual con-formation, but as it is relatively weakly resolved, its precise analysis is difficult. The loop F region has low sequence conservation in the nicotinic family (Fig. 1), and in other superfamily members it may have a different conformation, providing different residues to the binding site. Such changes could lead to variations in affinity, for example by changing the size of the ligand-binding site or its access route.

Close to the loop F region, the electron density was interpreted as a calcium ion, because the crystals were grown in the presence of Ca^{2+}. The cation has Asp B161, Asp B175 and the main chain of B176 as ligands. This putative Ca^{2+} ion may help to orientate Tyr B164 and could thus be involved in ligand binding. This agrees with observations that the residue equivalent to Asp B161 in muscle/*Torpedo* subunits (γAsp 174/δAsp 180) is important in ligand binding[14,15]. Additionally, calcium-binding sites that enhance the response to agonist binding have been identified in a homo-logous region (residue range 161–172) of the neuronal α_7-receptor[33].

The most likely access routes to the ligand-binding sites are from above or below the double-cysteine-containing loop C (Fig. 4a). This region buries the ligand-binding site from the solvent, pre-venting access from the outside. Access of some of the larger ligands, such as *d*-tubocurarine, would require the binding site to be opened up, for example by movement of the β-hairpin $\beta9$–$\beta10$ in the C-loop region. Access from the central pore has been suggested[21], but this would require major structural rearrangements at the interface, which are less likely.

From the location of the ligand-binding site, we can draw conclusions about the arrangement of ligand-binding α_1-subunits with respect to their complementary partners in the *Torpedo* and muscle receptors. It has been suggested that the $\alpha_1\gamma$ and $\alpha_1\delta$ interfaces occur in a clockwise $\alpha_1\gamma\alpha_1\delta\beta_1$ arrangement when looking towards the membrane[34]. Our structure would favour an anti-clockwise $\alpha_1\gamma\alpha_1\delta\beta_1$ arrangement, as the principal ligand-binding site is located on the anticlockwise side of its complementary partner (Fig. 2).

Ligand binding

To our surprise we found features of bulky electron density that stacked onto Trp 143 in each ligand-binding site in the experimental cross-crystal averaged electron density (Fig. 4b). We have assigned this to a HEPES (*N*-2-hydroxyethylpiperazine-*N*′-2-ethanesulpho-nic acid) buffer molecule, which contains a positively charged quaternary ammonium group and therefore has some similarity to known nicotinic receptor ligands. Its dissociation constant of 100 mM (data not shown) indicates that binding under crystal-lization conditions (100–150 mM) is possible at low occupancy.
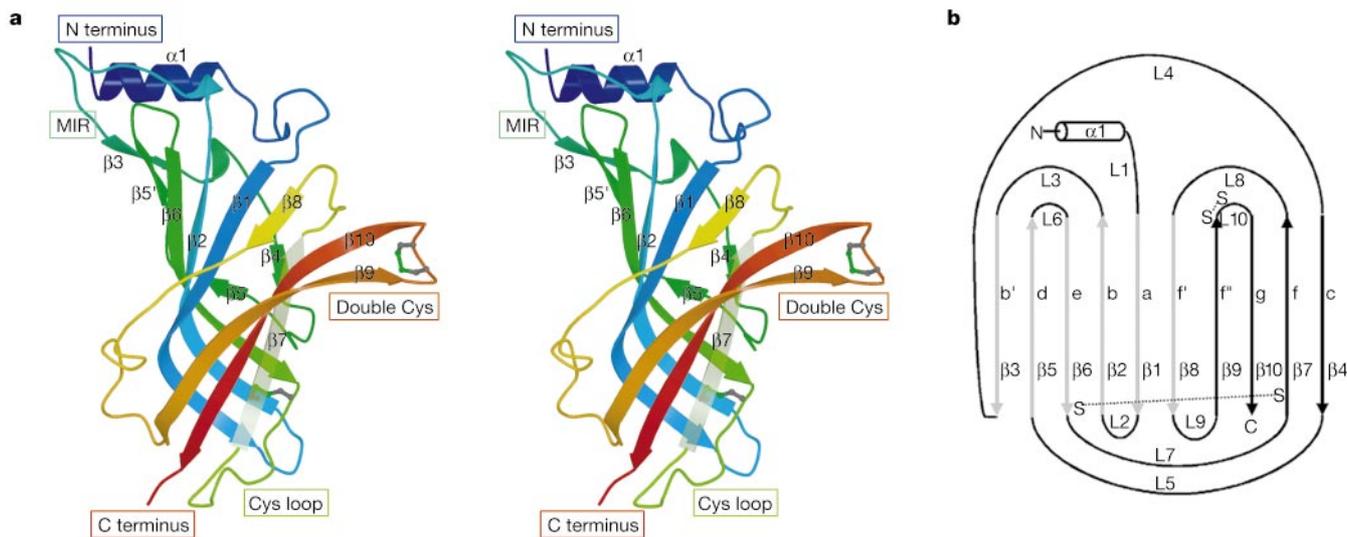
Figure 3 Overview of the AChBP protomer structure. **a**, Stereo representation of the AChBP protomer as viewed from outside the pentameric ring. This ribbon representation is coloured as a rainbow gradient, from blue (N terminus) to red (C terminus). Disulphide bridges are indicated in green ball-and-stick representation. In a complete ion channel the N terminus would point towards the synaptic cleft and the C terminus would enter the membrane at the bottom, continuing into the first transmembrane domain. **b**, Topology diagram of the AChBP protomer. For comparison with Ig-folds the strands have been labelled a–g, showing the additional strand (b′) and hairpin (f′–f″). In this structure, strands have been labelled $\beta1$–$\beta10$ with loops (or turns) L1–L10 preceding each strand with the same number. The $\beta5$ strand is broken ($\beta5$–$\beta5$′) with internal loop L5′; $\beta6$ also has a small break, but it is shown continuously (see Fig. 1). The precise beginnings and ends of strands may change slightly with increasing resolution, but the topology seen here will be highly conserved across the entire family of pentameric LGICs. S: disulphide bridge.

Although HEPES does not make any specific hydrogen bonds with the protein, it stacks with its quaternary ammonium onto Trp 143, making cation-π interactions as expected for nicotinic agonists[17,35] (Fig. 4b). It buries equal amounts of surface of the principal and complementary subunit. However, owing to low occupancy and limited resolution of the data, the precise orientation of the HEPES molecule cannot be definitely resolved. It has been suggested[3] that the ligand-binding site of nAChRs could be similar to that of acetylcholinesterase (AChE). Although the size of the binding site is roughly similar in AChBP and AChE, the observed arrangement of aromatic residues is quite different. However, the stacking of the quaternary ammonium of HEPES, as far as it can be refined in the current AChBP structure, is similar to that of the quaternary ammonium of the decamethonium in AChE on Trp 84 (ref. 36).

Pentamer interface
The subunit interface consists on the plus side entirely of loop regions (L1, L2, L4, L5, L7, L8 and L10), whereas the minus side mostly presents secondary structure elements to the interface (α1,

β1, β2, β3, β5, β6 and L9; Fig. 5). Several residues are important for both ligand binding and pentamer formation. The interface buries a large surface area (2,700 Å^2), with a mainly uncharged character including only a single bifurcated salt bridge (Glu A149–Arg B3 and Arg B104). It is a very convoluted surface, indicating that shape complementarity may be important in pentamer formation (Fig. 5a). The interface residues are not well conserved between subfamilies of the superfamily of pentameric ligand-gated ion channels (Fig. 1). The residues change markedly between the different ion-channel subtypes, with for example changes from hydrophobic to charged and vice versa (Fig. 1).

Ligand-gated ion channels
The superfamily of ligand-gated ion channels has highly conserved LBDs, and the function and location of the conserved residues can now be analysed in the light of the structure. Most residues that are conserved in the superfamily (Fig. 1) are hydrophobic and help to maintain the hydrophobic core of the protomer, grouped into three clusters (Fig. 6). The first cluster is involved in packing of
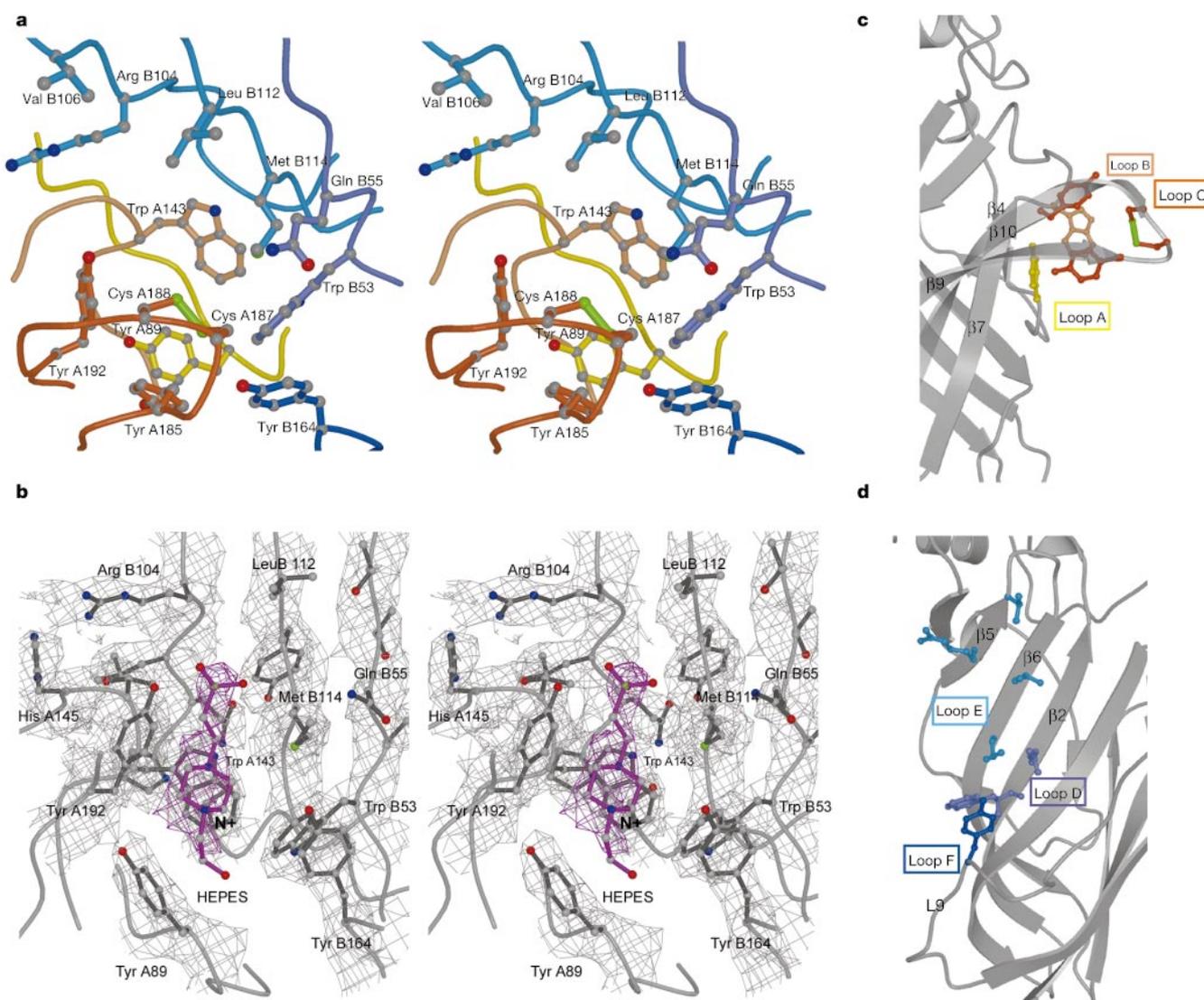
Figure 4 The ligand-binding site. **a**, Stereo representation of the ligand-binding site in ball-and-stick representation, showing the contribution of the principal 'loops': A (Tyr A89/α_1 Tyr 93, yellow), B (Trp A143/α_1 Trp 149, dark yellow) and C (Tyr A185/α_1 Tyr 190, Cys A187/α_1 Cys 192, Cys A188/α_1 Cys 193, Tyr A192/α_1 Tyr 198, orange), and the complementary 'loops' D (Trp B53/γ Trp 55, Gln B55/γGlu 57, violet), E (Arg B104/γLeu 109, Val B106/γTyr 111, Leu B112/γTyr 117, Met B114/γLeu 119,

light blue) and F (Tyr B164, blue). **b**, Stereo view of the electron density map displaying a HEPES buffer molecule in the ligand-binding site. This experimental density (contoured at 1 σ) is derived from cross-crystal averaging. **c**, Location of the principal ligand-binding residues (colours as in **a**, orientation as in Fig. 2b). **d**, Location of the complementary ligand-binding residues (colours as in **a**, orientation as in Fig. 2b). Note that loops D, E and F are all on β-strands.
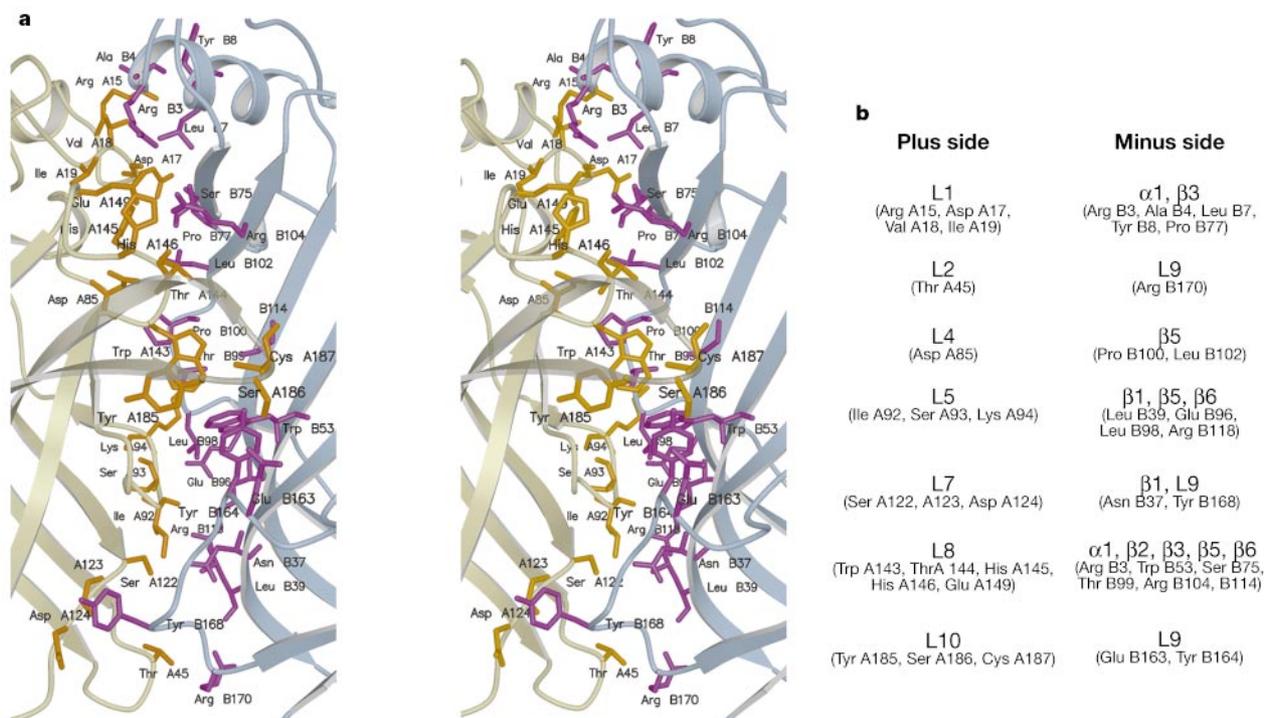
Figure 5 Dimer interface. **a**, Stereo figure of the dimer interface. Representation of the interface residues (ball-and-stick) on a schematic secondary structure. The figure shows the plus face of subunit A (light yellow, orange interface residues) and the minus face of subunit B (light blue, pink interface side chains). **b**, Dimer interface interactions. Note that owing to the low conservation of these interfaces (Fig. 1) the actual interactions will not be conserved in any pentameric LGIC interface, but that in all receptors these topological regions are likely to form the interface.

the N-terminal helix α1 against the main framework of the proto-mer. The second cluster is situated in the upper half of the β-core region. The third cluster is located at the lower end of the β-sandwich (Fig. 6). In the superfamily, two residues are conserved in the ligand-binding site. Only very few conserved residues are hydrophilic; two of these maintain the turns of a Greek key motif connecting strands β3, β5, β6 and β2, in which Asp 60 stabilizes the N terminus of a small 3₁₀ helix and Gly 109 enables tight-turn formation. Conserved residues Asp 85 and Asn 90 are involved in packing of the β-sheets. Asp 85 forms hydrogen bonds to the highly conserved Ser 142 and Thr 144, and residue Asn 90 brings together the main-chain oxygens of Ser 122 and Arg 137, enabling disulphide-bond formation of the nearby absolutely conserved disulphide bond (123–136). This disulphide bond is topologically equivalent to the 'tyrosine cornerstone'[37] found in Ig-like proteins, in which tyrosine links the two β-sheets together, and a similar role is fulfilled by the disulphide bond in AChBP. This structural role for the disulphide bond explains why, in the *Torpedo* receptor, the Cys 128–Cys 142 bond is important for both preservation of subunit conformational stability[38] and complete nAChR assembly[39]. As the conserved residues mainly contribute to the overall structure formation, it is clear that all pentameric LGIC N-terminal domains will have the same three-dimensional structure.

Contrary to the above residues, the Cys loop (Fig. 3a) is well conserved in the pentameric LGIC family but not in AChBP (Fig. 1, residues 129–141). It is hydrophobic in the receptors, whereas it is hydrophilic in AChBP. The Cys loop is located at the bottom (membrane) side of the protein, close to the dimer interface. This position, and its hydrophobicity in the LGIC family, implies that it could interact with the membrane or with the transmembrane region of the receptors, functions that are absent in AChBP.

Finally, the interface region is among the least conserved regions in the superfamily (Fig. 1). Pentamer formation does not apparently impose very stringent evolutionary requirements on these domains.
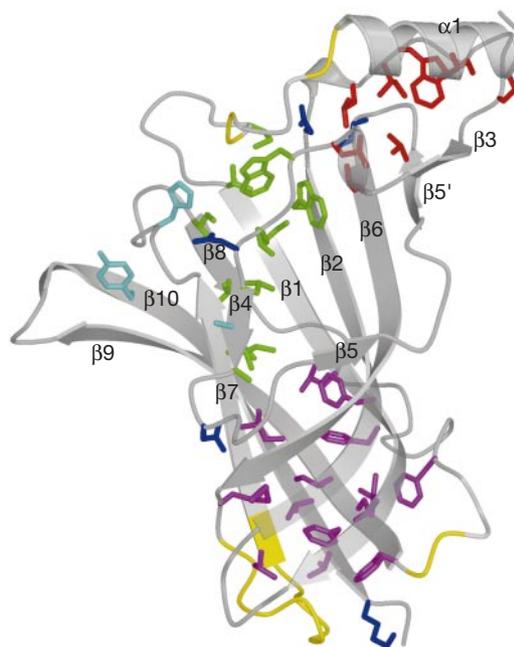
Figure 6 Conservation in the pentameric LGIC superfamily. Conserved residues are indicated as viewed from the central pore. Hydrophobic cluster I (red): residues 6, 10, 63, 65, 71, 81, 105, 111; Cluster II (green): residues 20, 27, 29, 58, 82, 84, 86, 88, 140, 150, 152, 195; Cluster III (pink): residues 33, 35, 38, 41, 48, 52, 123, 125, 136, 138, 165, 171, 173, 199, 201. The hydrophilic conserved residues (dark blue): Asp 60, Asp 85, Asn 90, Gly 109, Lys 203. Conserved residues in the ligand-binding site (light blue): His 145, Tyr 192, or close by: Ala 87. Very few conserved residues are at the surface. Residues conserved between pentameric LGICs but not AChBP are indicated by yellow main chain (14, 19, 170 and the Cys-loop124–135).

The high level of structural conservation, however, implies that the same topological regions form these interface contacts in all superfamily members (Fig. 5b). But in these interfaces different combinations of subunits will have different interactions, possibly creating variations in the precise allosteric contacts and movements in the various subclasses of these ion channels.

Activation mechanism

The location of the ligand-binding site is conserved among pentameric LGIC receptors[1] but the actual ligand-binding residues vary, creating specificity for different ligands. However, all ligand-gated ion channel LBDs have intrinsically the same function: the activation of a membrane pore. Indeed, a nicotinic receptor LBD is capable of activating a serotonin membrane channel in a chimaeric receptor[40]. Thus, the essential activation mechanism is conserved across the superfamily. One option is that activation takes place by direct rotation of the protomer through a pivoting point at the ligand-binding site. But for any other mechanism, the location of the conserved residues implies that transmission of a signal from the binding pocket to the transmembrane domain takes place within the protomer and not through the interface region.

Within the protomer, several possible regions could transmit activation signals: changes in loop C, induced by ligand binding, could be transmitted directly into the transmembrane domain through the $\beta9-\beta10$ β-hairpin; alternatively, large structural changes in the β-sheet regions could be transmitting the signal through the conserved Cys loop, acting directly on the membrane part of the pentameric LGICs. The movement observed at 9 Å for the *Torpedo* nAChR upon agonist binding[19] fits well with the latter suggestion. We see a twisted β-sandwich, with two distinct hydrophobic cores, and it is possible that these cores move with respect to each other upon ligand binding. The effect of any of these activation mechanisms in the protomer will then be modulated by the varying subunit interfaces in the different subtypes of the receptor, allowing intricate specificity in neuronal signal transmission.

Conclusions

This crystal structure shows that molluscan AChBP is a homologue of the pentameric LGIC superfamily ligand-binding domains. It confirms the predicted Ig-topology, the location of the binding site at the subunit interface, the position of the MIR and the extensive data on the nicotinic ligand-binding residues.

With this structure, we present the first detailed three-dimensional information about the fold and the arrangement of the nicotinic ligand-binding site. It also clarifies the arrangement of subunits in nicotinic muscle receptors by showing the relative positioning of the principal and complementary part of the ligand-binding site.

The AChBP crystal structure provides an explanation for the role of the pentameric LGIC superfamily conserved residues. They stabilize the protomer structure by the formation of hydrophobic cores and packing of secondary structure elements. The crystal structure clarifies how the LGIC pentamers are built up, and how weakly the pentamer interfaces are conserved between LGICs, which has implications for the modes of action.

It is unclear whether AChBP performs the allosteric and desensitization movements that are important for pentameric LGIC function. AChBP is a soluble protein with a natural role in the modulation of synaptic transmission and lacks a transmembrane channel[27]. Thus, ligand binding does not result in opening of a pore in AChBP, although some of the movements could be conserved in its evolution. Similarly, it is unclear whether non-competitive antagonist-binding sites are present in AChBP. Such questions can be addressed with chimaeric molecules and possibly by further crystallographic studies.

This structure will be highly relevant for the numerous drug-design studies that are targeting the pentameric LGIC superfamily.

The general structural knowledge on its folding will be applicable to the GABA, serotonin (5-HT$_3$) and glycine receptor fields. It will help us to understand their ligand-binding characteristics and hence could have an impact on the development of, for example, anti-emetics aimed at the 5-HT$_3$ receptor or the mood-defining drugs that target the GABA receptors. The availability of a three-dimensional description of the nicotinic ligand-binding site will be especially relevant for the design of new drugs against, for example, Alzheimer's disease, epilepsy and addiction to smoking. □

Methods

Protein purification

AChBP was cloned into expression vector pPIC9 (without residue Leu 1) and over-expressed in yeast, *Pichia pastoris* GS115, according to the Invitrogen manual. After 4 days of induction the medium was collected, concentrated and dialysed against standard buffer (20 mM Tris–HCl buffer (pH 8.0), 150 mM NaCl and 0.02% (w/v) NaN$_3$). The protein was purified by anion exchange (Poros50 HQ, MonoQ), and gel filtration (Superdex 200). It was dialysed against 50 mM HEPES buffer (pH 7.0) with 0.02% NaN$_3$ and concentrated to ~20 mg ml^{-1}. N-terminal sequencing revealed that part of the pPIC9-encoded signal sequence is retained, before residue 2 (sequence EAEAYVEF). The experimental relative molecular mass was 26,544 (MALDI), ~2K more than the calculated mass based on the sequence (24,649), owing to glycosylation at position Asn 66, as confirmed by deglycosylation experiments (data not shown).

Crystallization

We grew the crystals at room temperature using the hanging-drop vapour diffusion technique. All drops contained 2 µl of protein (10 mg ml^{-1}) and 2 µl of reservoir solution (9–11% (w/v) PEG 4000, 100 mM HEPES (pH 7.0), 50–200 mM CaCl$_2$ and 0.02% NaN$_3$). Depending on the batch of protein and the CaCl$_2$ concentration, we obtained three crystal forms. Orthorhombic and monoclinic crystals appeared under high CaCl$_2$ concentration and were frequently twinned. The orthorhombic crystals ($P2_12_12_1$) have the following cell constants: $a = 120.6$ Å, $b = 137.0$ Å, $c = 161.5$ Å, with two pentamer molecules per asymmetric unit (asu). The monoclinic crystals ($P2_1$) are very similar in morphology to the orthorhombic ones, but gave lower resolution data (~3.3 Å), with the following cell constants: $a = 121.1$ Å, $b = 162.1$ Å, $c = 139.4$ Å, $\beta = 90.13°$, and four pentamers per asu. The tetragonal crystal form ($P4_22_12$) was obtained from a solution containing 11.5 (w/v) PEG 4000, 100 mM HEPES (pH 7.0), 150 mM CaCl$_2$ and 0.02% (w/v) NaN$_3$. They have the following cell constants: $a = b = 141.66$ Å, $c = 120.83$ Å and one pentamer per asu. For MAD experiments, orthorhombic and monoclinic crystals were soaked in mother liquor solution containing 5 mM and 10 mM trimethyl-lead acetate (MePb) respectively for 5 days. Before flash-cooling, all crystals were gradually equilibrated against mother liquor with 30% glycerol.

In all three space groups AChBP forms a decamer structure with 52 symmetry, where 2 pentamers have contact with each other through a calcium-binding site, at the 'top' of the α1 helix. This binding site (Asp 2 and Asp 5 from two protomers) is not conserved in the pentameric LGIC family. In the tetragonal space group the two-fold of the decamer coincides with a crystallographic two-fold. In solution, the AChBP protein behaves as a pentamer[27].

Structure determination and refinement

We collected native data (X11) and the Pb-1 data sets (BW7A) at the EMBL outstation at the DESY synchrotron in Hamburg and the Pb-2 data sets (BM14) at the ESRF, Grenoble (Table 1). Data were processed with DENZO/SCALEPACK[41] (native) or MOSFLM[42]/SCALA[43] software (Pb-1, Pb-2). The Pb sites, located at the interface of two pentamers, were found for both MAD sets by SOLVE[44] and heavy atom parameters were optimized with SHARP[45]. NCS operators were found and refined with NCS6D and IMP[46]. Multi-crystal averaging was executed with DM-multi[47] using amplitudes from the monoclinic, orthorhombic and native (tetragonal) data sets, and experimental phases from the orthorhombic and monoclinic MAD experiments. The model was built in O[48] and refined with CNS[49], against the tetragonal 2.7 Å data. Refinement included partial fivefold NCS restraints, an overall anisotropic B factor and bulk solvent correction. The unusual vicinal disulphide bridge[8], Cys 187–Cys 188, was visible in the electron density, but because of the limited resolution it was not analysed in detail. The final model contains 1,025 residues of AChBP pentamer, 5 HEPES molecules, 10 Ca^{2+} ions and 15 water molecules. The entire AChBP pentamer is well ordered, except for the N-terminus seven residues (part of the signal sequence) and the last five C-terminal residues. In addition, the HEPES, loop region 155–160 and the sugar residues attached to residue Asn 66 are not well resolved in the electron density. Root-mean-square deviations from ideal geometry for bond distances and angles are 0.01 Å and 1.6°, respectively.

1. Ortells, M. O. & Lunt, G. G. Evolutionary history of the ligand-gated ion-channel superfamily of receptors. *Trends Neurosci.* **18,** 121–127 (1995).
2. Corringer, P. J., Le Novère, N. & Changeux, J. P. Nicotinic receptors at the amino-acid level. *Annu. Rev. Pharmacol. Toxicol.* **40,** 431–458 (2000).
3. Changeux, J. P. & Edelstein, S. J. Allosteric receptors after 30 years. *Neuron* **21,** 959–980 (1998).
4. Arias, H. R. Localization of agonist and competitive antagonist binding sites on nicotinic acetylcholine receptors. *Neurochem. Int.* **36,** 595–645 (2000).

5. Paterson, D. & Nordberg, A. Neuronal nicotinic receptors in the human brain. *Prog. Neurobiol.* **61**, 75–111 (2000).

6. Galzi, J. L. *et al.* Identification of a novel amino acid alpha-tyrosine 93 within the cholinergic ligands-binding sites of the acetylcholine receptor by photoaffinity labeling. Additional evidence for a three-loop model of the cholinergic ligands-binding sites. *J. Biol. Chem.* **265**, 10430–10437 (1990).

7. Dennis, M. *et al.* Amino acids of the *Torpedo marmorata* acetylcholine receptor alpha subunit labeled by a photoaffinity ligand for the acetylcholine binding site. *Biochemistry* **27**, 2346–2357 (1988).

8. Kao, P. N. & Karlin, A. Acetylcholine receptor binding site contains a disulfide cross-link between adjacent half-cystinyl residues. *J. Biol. Chem.* **261**, 8085–8088 (1986).

9. Middleton, R. E. & Cohen, J. B. Mapping of the acetylcholine binding site of the nicotinic acetyl-choline receptor: [3H]nicotine as an agonist photoaffinity label. *Biochemistry* **30**, 6987–6997 (1991).

10. Fu, D. X. & Sine, S. M. Competitive antagonists bridge the alpha-gamma subunit interface of the acetylcholine receptor through quaternary ammonium-aromatic interactions. *J. Biol. Chem.* **269**, 26152–26157 (1994).

11. O'Leary, M. E., Filatov, G. N. & White, M. M. Characterization of *d*-tubocurarine binding site of *Torpedo* acetylcholine receptor. *Am. J. Physiol.* **266**, C648–653 (1994).

12. Corringer, P. J. *et al.* Identification of a new component of the agonist binding site of the nicotinic alpha 7 homo-oligomeric receptor. *J. Biol. Chem.* **270**, 11749–11752 (1995).

13. Sine, S. M., Kreienkamp, H. J., Bren, N., Maeda, R. & Taylor, P. Molecular dissection of subunit interfaces in the acetylcholine receptor: identification of determinants of alpha-conotoxin M1 selectivity. *Neuron* **15**, 205–211 (1995).

14. Czajkowski, C., Kaufmann, C. & Karlin, A. Negatively charged amino-acid residues in the nicotinic receptor delta subunit that contribute to the binding of acetylcholine. *Proc. Natl Acad. Sci. USA* **90**, 6285–6289 (1993).

15. Martin, M., Czajkowski, C. & Karlin, A. The contributions of aspartyl residues in the acetylcholine receptor gamma and delta subunits to the binding of agonists and competitive antagonists. *J. Biol. Chem.* **271**, 13497–13503 (1996).

16. Prince, R. J. & Sine, S. M. Molecular dissection of subunit interfaces in the acetylcholine receptor. Identification of residues that determine agonist selectivity. *J. Biol. Chem.* **271**, 25770–25777 (1996).

17. Dougherty, D. A. Cation-pi interactions in chemistry and biology: a new view of benzene, Phe, Tyr, and Trp. *Science* **271**, 163–168 (1996).

18. Unwin, N. Nicotinic acetylcholine receptor at 9 Å resolution. *J. Mol. Biol.* **229**, 1101–1124 (1993).

19. Unwin, N. Acetylcholine receptor channel imaged in the open state. *Nature* **373**, 37–43 (1995).

20. Beroukhim, R. & Unwin, N. Three-dimensional location of the main immunogenic region of the acetylcholine receptor. *Neuron* **15**, 323–331 (1995).

21. Miyazawa, A., Fujiyoshi, Y., Stowell, M. & Unwin, N. Nicotinic acetylcholine receptor at 4.6 Å resolution: transverse tunnels in the channel wall. *J. Mol. Biol.* **288**, 765–786 (1999).

22. West, A. P. Jr, Bjorkman, P. J., Dougherty, D. A. & Lester, H. A. Expression and circular dichroism studies of the extracellular domain of the alpha subunit of the nicotinic acetylcholine receptor. *J. Biol. Chem.* **272**, 25468–25473 (1997).

23. Schrattenholz, A. *et al.* Expression and renaturation of the N-terminal extracellular domain of *Torpedo* nicotinic acetylcholine receptor alpha-subunit. *J. Biol. Chem.* **273**, 32393–32399 (1998).

24. Alexeev, T. *et al.* Physicochemical and immunological studies of the N-terminal domain of the *Torpedo* acetylcholine receptor alpha-subunit expressed in *Escherichia coli*. *Eur. J. Biochem.* **259**, 310–319 (1999).

25. Wells, G. B., Anand, R., Wang, F. & Lindstrom, J. Water-soluble nicotinic acetylcholine receptor formed by alpha7 subunit extracellular domains. *J. Biol. Chem.* **273**, 964–973 (1998).

26. Tierney, M. L. & Unwin, N. Electron microscopic evidence for the assembly of soluble pentameric extracellular domains of the nicotinic acetylcholine receptor. *J. Mol. Biol.* **303**, 185–196 (2000).

27. Smit, A. B. *et al.* A glia-derived acetylcholine-binding protein that modulates synaptic transmission. *Nature* **411**, 261–268 (2001).

28. Bork, P., Holm, L. & Sander, C. The immunoglobulin fold. Structural classification, sequence patterns and common core. *J. Mol. Biol.* **242**, 309–320 (1994).

29. Le Novère, N., Corringer, P. J. & Changeux, J. P. Improved secondary structure predictions for a nicotinic receptor subunit: incorporation of solvent accessibility and experimental data into a two-dimensional representation. *Biophys. J.* **76**, 2329–2345 (1999).

30. Holm, L. & Sander, C. Dali/FSSP classification of three-dimensional protein folds. *Nucleic Acids Res.* **25**, 231–234 (1997).

31. Tzartos, S. J. *et al.* The main immunogenic region (MIR) of the nicotinic acetylcholine receptor and the anti-MIR antibodies. *Mol. Neurobiol.* **5**, 1–29 (1991).

32. Fernando Valenzuela, C., Weign, P., Yguarabide, J. & Johnson, D. A. Transverse distance between the membrane and the agonist binding sites on the *Torpedo* acetylcholine receptor: a fluorescence study. *Biophys. J.* **66**, 674–682 (1994).

33. Galzi, J. L., Bertrand, S., Corringer, P. J., Changeux, J. P. & Bertrand, D. Identification of calcium binding sites that regulate potentiation of a neuronal nicotinic acetylcholine receptor. *EMBO J.* **15**, 5824–5832 (1996).

34. Machold, J., Weise, C., Utkin, Y., Tsetlin, V. & Hucho, F. The handedness of the subunit arrangement of the nicotinic acetylcholine receptor from *Torpedo californica*. *Eur. J. Biochem.* **234**, 427–430 (1995).

35. Zhong, W. *et al.* From ab initio quantum mechanics to molecular neurobiology: a cation-pi binding site in the nicotinic receptor. *Proc. Natl Acad. Sci. USA* **95**, 12088–12093 (1998).

36. Harel, M. *et al.* Quaternary ligand binding to aromatic residues in the active-site gorge of acetylcholinesterase. *Proc. Natl Acad. Sci. USA* **90**, 9031–9035 (1993).

37. Hemmingsen, J. M., Gernert, K. M., Richardson, J. S. & Richardson, D. C. The tyrosine corner: a feature of most Greek key beta-barrel proteins. *Protein Sci.* **3**, 1927–1937 (1994).

38. Mishina, M. *et al.* Location of functional regions of acetylcholine receptor α-subunit by site-directed mutagenesis. *Nature* **313**, 364–369 (1985).

39. Green, W. N. & Wanamaker, C. P. Formation of the nicotinic acetylcholine receptor binding sites. *J. Neurosci.* **18**, 5555–5564 (1998).

40. Eisele, J. L. *et al.* Chimaeric nicotinic-serotonergic receptor combines distinct ligand binding and channel specificities. *Nature* **366**, 479–483 (1993).

41. Otwinowski, Z. & Minor, W. Processing of X-ray diffraction data collected in oscillation mode. *Methods Enzymol.* **276**, 307–326 (1997).

42. Leslie, A. G. Integration of macromolecular diffraction data. *Acta Crystallogr. D Biol. Crystallogr.* **55**, 1696–1702 (1999).

43. Collaborative Computational Project, Number 4. The *CCP4* suite: programs for protein crystal-lography. *Acta Crystallogr. D* **50**, 760–763 (1994).

44. Terwilliger, T. C. & Berendzen, J. Automated MAD and MIR structure solution. *Acta Crystallogr. D Biol. Crystallogr.* **55**, 849–861 (1999).

45. La Fortelle, E. de & Bricogne, G. Maximum-likelihood heavy-atom parameter refinement in the MIR and MAD methods. *Methods Enzymol.* **276**, 472–494 (1997).

46. Kleywegt, G. J. & Jones, T. A. in *From First Map to Final Model* (eds Bailey, S., Hubbard, R. & Waller, D.) 59–66 (SERC Daresbury Laboratory, Warrington, 1994).

47. Cowtan, K. *Joint CCP4 and ESF-EACBM Newsletter on Protein Crystallography* **31**, 34–38 (1994).

48. Jones, T. A., Zou, J-Y., Cowan, S. W. & Kjeldgaard, M. Improved methods for building protein models in electron density maps and the location of errors in these models. *Acta Crystallogr. A* **47**, 110–119 (1991).

49. Brünger, A. T. *et al.* Crystallography & NMR system: A new software suite for macromolecular structure determination. *Acta Crystallogr. D* **54**, 905–921 (1998).

50. Thompson, J. D., Gibson, T. J., Plewniak, F., Jeanmougin, F. & Higgins, D. G. The CLUSTAL_X windows interface: flexible strategies for multiple sequence alignment aided by quality analysis tools. *Nucleic Acids Res.* **25**, 4876–4882 (1997).